ARMY RESEARCH LABORATORY

Computational Method for Atomistic-Continuum Homogenization

by Peter W. Chung, Raju R. Namburu, Charles Cornwell,
Brian J. Henz, and Jerry A. Clarke

ARL-TR-2894 December 2002

NOTICES

Disclaimers

The findings in this report are not to be construed as an official Department of the Army position unless so designated by other authorized documents.

Citation of manufacturer's or trade names does not constitute an official endorsement or approval of the use thereof.

Destroy this report when it is no longer needed. Do not return it to the originator.

Army Research Laboratory
Aberdeen Proving Ground, MD 21005-5067

ARL-TR-2894 **December 2002**

Computational Method for Atomistic-Continuum Homogenization

Peter W. Chung, Raju R. Namburu, Brian J. Henz, and Jerry A. Clarke
Computational and Information Sciences Directorate, ARL

Charles Cornwell
High Performance Technologies, Inc.

Acknowledgments

This work was funded through the U. S. Army Research Laboratory Director's Research Initiative Program under award number FY02-CIS-01. We gratefully acknowledge this support.

Table of Contents

List of Figures

List of Tables

INTENTIONALLY LEFT BLANK.

1. Introduction

A large amount of research interest has focused on the multiscale problem involving atoms and continua. It is widely accepted that many effects on the continuum germinate at the atomic level. Events such as fracture, fatigue, and inelastic material response can be traced back to phenomena in the atomic structure. Moreover, fabrication of nanoscale devices in mass quantities will likely come from nanopatterning techniques (e.g., see [1]). Creating patterns at the nanometer scale will likely involve unforeseen effects when coupled to mechanical loads. Therefore, a computational mechanics method is necessary that can couple disparate scales – one scale in which the boundary conditions are applied and the other in which atoms reside.

Nanopatterning has recently become popular for creating organized nanostructured materials, which are those that may be defined as materials whose structural elements, clusters, crystallites and molecules have dimensions in the 1- to 100-nm range. Experimental methods can be designed to exploit the symmetries and repetitiveness of periodic nanostructures to control the environment in which ultra-thin films and surfaces are created. Periodic structures are often desireable because, when atoms and electrons are confined within nanoscale semiconductors and metal clusters, unique properties arise. Such materials are formed under a different paradigm of "bottom up" instead of conventional "top down" techniques. Figures 1 and 2, respectively, illustrate some recent work of experimental and numerical nanopatterning. In performing rigorous analysis of such systems, the impact of mechanical stresses and strains on the evolution and characteristics of the atoms must be modeled carefully. This requires a technique for translating mechanical information at the boundaries, e.g., clamps, pin joints, and loads, down to the atomic level. Moreover, to ensure that the mechanical nature of the problem stays consistent with the atomistic problem, the information contained at the atomic level must be transferred back up.

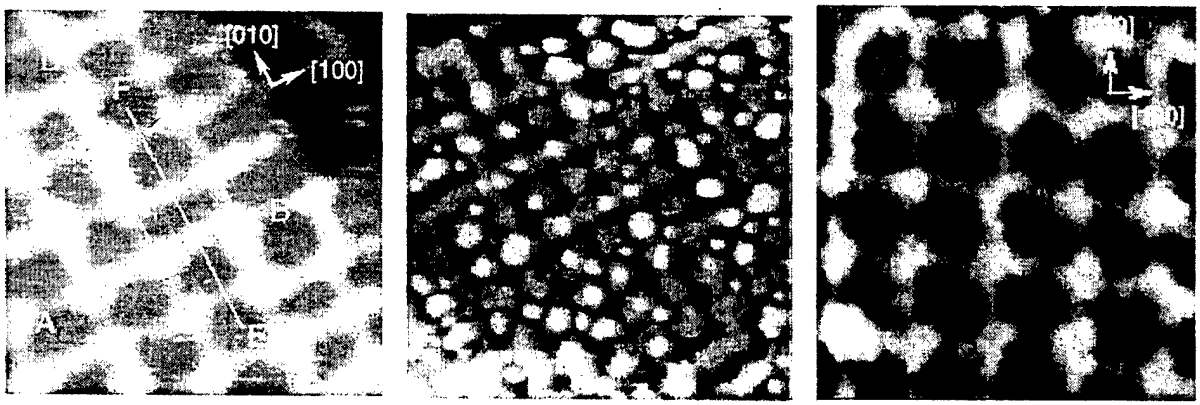

(a) Array of nitrogen-modified copper nanodots (dark patches) and clean copper lines (bright areas).

(b) Cobalt grown on the copper-nitrogen nanodot surface.

(c) Iron deposited on the copper-nitrogen nanodot surface.

Figure 1. Scanning tunneling microscopy (STM) images of experimental nanopatterned systems [2].

Methodologies for linking a continuum to an atomistic domain can be found in literature as early 1971 [4]. Finite element (FE) methods were later employed in Mullins and Dokainish [5] using a numerically decoupled domain approach with spatially overlapping atomistic and continuum regions. A review of some of these methods can be found by Cleri et al. [6]. Among these early analytic and computational studies, frequent issues regarding the treatment of the interface arose, which were primarily handled through creative use of kinematic constraints. For example, Tadmor et al. [7] developed an FE-based formulation, the so-called quasicontinuum method. Similar efforts were made through the so-called handshaking or coupling-of-length-scales (CLS) method by Broughton et al. [8] by increasing the atomic resolution to account for electron degrees of freedom via the tight-binding (TB) method. The dynamic problem was studied with a generalized scaling approach in coarse-grained molecular dynamics (CGMD) by Rudd and Broughton [9] to better handle the propagation of waves through the atomistic-FE interface and the FE far field.

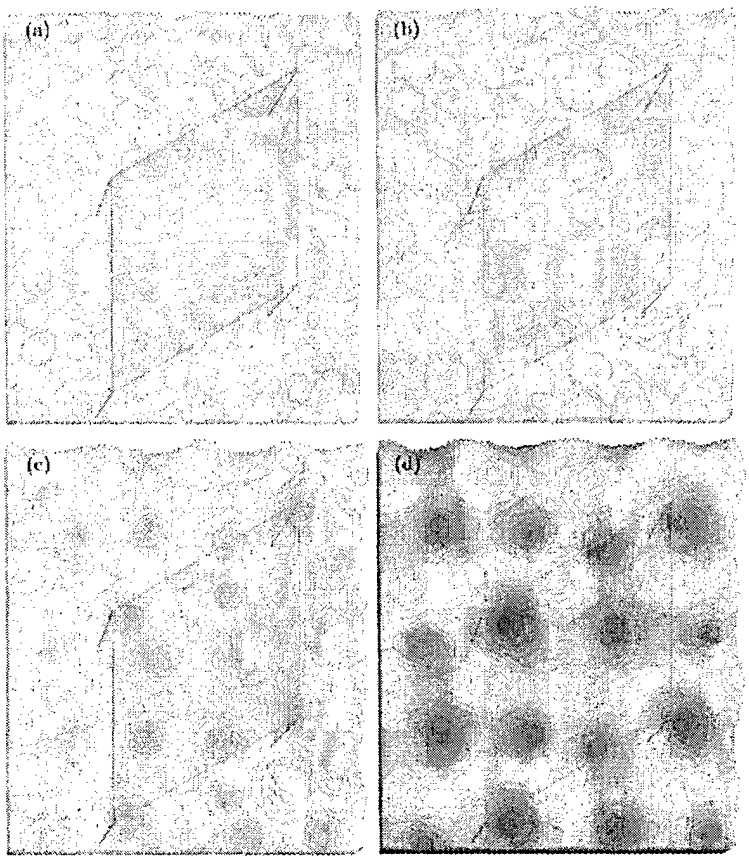

Figure 2. Monte Carlo numerical simulation of ion erosion of platinum (111) surface. The darker diamond region is the periodic cell and darkened pit-regions are areas of greater depth. (a)–(d) illustrate removal of mono-layers by ion erosion, each of greater depth [3].

Multiscale methods such as these have traditionally been limited mainly to localized regions of interest. For example, the applications to which these methods have been applied involve small sets of dislocations and cracks and limited analyses of their mutual interactions. The localized regions on which these simulations are run typically span, at most, several microns because of the bottleneck imposed by a direct interface between the continuum region and atomistic region. To ensure compatibility, kinematic constraints are used to tie together the equations and disparate length scales across this interface. Driving the resolution of the discretized continuum down to the atom scale to accommodate the interface intrinsically

restricts the size of the continuum and leads to smaller overall dimensions of the problem. This can only be overcome by larger use of computer resources when dealing with problems with larger dimensions.

The asymptotic expansion homogenization method has been widely studied by applied mathematicians for many years. Numerous texts on the basic theory can be found in the literature, for instance, by Bensoussan et al. [10], Sanchez-Palencia [11], and Bakhvalov and Panasenko [12]. Yet, despite the prolific research in the field, no attempts have been documented for extending the technique to atoms.

Homogenization may be particularly suited for nanopatterned systems because of the use of periodicity and asymptotics in the assumptions, perhaps even more so than traditional materials that employ homogenization theory such as composites. This is because, in most cases, the ratio of scales in atomistic-continuum problems better represents the asymptotic assumption in homogenization than in other types of multiscale problems. Furthermore, the periodic nature of nanopatterned systems is more apt at realistically adhering to the periodic assumption than unit cell models of composite material inclusions.

In this report, the progress and initial results for a computational framework for homogenization of the atomistic problem is presented. Using two concurrent domains, one for the macroscale continuum domain and one for the periodic atomic scale domain, self-consistent sets of equations are derived. Atoms in arbitrary configurations and structures of unlimited size are permitted. Through the asymptotic expansion homogenization technique, a set of hierarchical equations are derived based on hyperelasticity. At the local level, the atomistic equations are used under the assumption of the harmonic approximation to generate the effective properties needed to solve the effective global level equations. The Cauchy-Born rule [13] is applied to the atoms to enforce the gross deformation of the continuum on the atoms. This circumvents the need to apply kinematic constraints by making use of the weak averaging properties of homogenization.

The outline of this report is as follows. In section 2, the conventional continuum equations are shown, eventually leading to a variational form based on the principle of virtual work. Then, in section 3, the multiscale equations are developed, resulting in two sets of equations that govern the local and global length scales. By introducing the atomistic potential in sections 4 and 5, the details of the atomistic formulations are presented and cast in a variational form for use in the multiscale homogenization method. In section 6, the derivatives of the atomistic energy potential needed to complete the derivation of the method are provided in a general form. In section 7, one- and two-dimensional (1-D and 2-D) demonstrative examples are shown. Closing remarks are discussed in section 8. Additional details of the analytical derivatives of the Tersoff-Brenner Type II potential were presented in [14].

2. Continuum Formulations

This section describes the kinematics, stress definitions, and linear momentum conservation laws needed to develop the homogenization method from atomistic principles.

2.1 Kinematics

Consider an open set V in $\Re^3$ that deforms to the configuration v in $\Re^3$. Points in V are denoted $\mathbf{X} = (X_1, X_2, X_3) \in V$ and are called material points, whereas points in v are denoted $\mathbf{x} = (x_1, x_2, x_3) \in v$ and are called spatial points. The deformation is a one-to-one mapping through $\boldsymbol{\phi}$ so that $x = \boldsymbol{\phi}(X)$. The deformation gradient is defined by

$$\mathbf{F} = \frac{\partial \boldsymbol{\phi}}{\partial \mathbf{X}} = \frac{\partial \mathbf{x}}{\partial \mathbf{X}} = \nabla_0 \mathbf{x} \quad \text{and} \quad F_{ij} = \frac{\partial \phi_i}{\partial X_j} = \frac{\partial x_i}{\partial X_j}, \tag{1}$$

where ∇_0 signifies the gradient taken with respect to V. The determinant of F is termed the Jacobian and is defined by $J = \det \mathbf{F}$. The right Cauchy-Green strain tensor is defined

by

$$\mathbf{C} = \mathbf{F}^T\mathbf{F}, \tag{2}$$

and the Green strain tensor is defined by

$$\mathbf{E} = \frac{1}{2}(\mathbf{C} - \mathbf{I}). \tag{3}$$

2.2 Stress and Equilibrium

The material representation for the conservation of linear momentum is defined by

$$\nabla_0 \cdot \mathbf{P} + \mathbf{f}_0 = 0, \tag{4}$$

where $\mathbf{P}$ is the first Piola-Kirchoff stress tensor and $\mathbf{f}_0$ is the body force per unit of undeformed volume. In rate form, it is given by

$$\nabla_0 \cdot \dot{\mathbf{P}} + \dot{\mathbf{f}}_0 = 0. \tag{5}$$

Using the principle of virtual work, equation (5) can be rewritten as

$$\int_V \left(\nabla_0 \cdot \dot{\mathbf{P}}\right) \delta\mathbf{u} dV + \int_V \dot{\mathbf{f}}_0 \cdot \delta\mathbf{u} dV = 0, \qquad \forall \delta\mathbf{u}, \tag{6}$$

where $\delta\mathbf{u}$ is the virtual displacement. Then, using the definition for traction with respect to the undeformed body, equation (6) can be rewritten as

$$\int_V \dot{\mathbf{P}} : \nabla_0 \delta\mathbf{u} dV = \int_{\partial V} \dot{\mathbf{t}}_0 \cdot \delta\mathbf{u} dA + \int_V \dot{\mathbf{f}}_0 \cdot \delta\mathbf{u} dV. \tag{7}$$

We invoke the notion of hyperelasticity by assuming that the atomistic potential, $\mathcal{W}$, which is a function of the atom positions, can be expressed in terms of strain. This assumes that the strain energy density (or the free energy at zero temperature) is equivalent to the atomistic

energy potential. Following classical continuum mechanics, one can then define the first Piola-Kirchoff stress as

$$\mathbf{P} = \frac{\partial \mathcal{W}}{\partial \mathbf{F}} \quad \text{and} \quad P_{ij} = \frac{\partial \mathcal{W}}{\partial F_{ij}}, \tag{8}$$

and the first Lagrangian elasticity tensor [15] as

$$\boldsymbol{\mathcal{C}} = \frac{\partial^2 \mathcal{W}}{\partial \mathbf{F} \partial \mathbf{F}} = \frac{\partial \mathbf{P}}{\partial \mathbf{F}} \quad \text{and} \quad \mathcal{C}_{ijkl} = \frac{\partial^2 \mathcal{W}}{\partial F_{ij} \partial F_{kl}} = \frac{\partial P_{ij}}{\partial F_{kl}}. \tag{9}$$

A relationship is needed between stress and strain. From equation (9), one can see that in hyperelastic materials, $\mathbf{P}$ is related to $\mathbf{F}$ through

$$\dot{\mathbf{P}} = \boldsymbol{\mathcal{C}} \dot{\mathbf{F}} \quad \text{and} \quad \dot{P}_{ij} = \mathcal{C}_{ijkl} \dot{F}_{kl}, \tag{10}$$

where

$$\dot{\mathbf{F}} = \partial \dot{\mathbf{u}} / \partial \mathbf{X} = \partial \mathbf{v} / \partial \mathbf{X}, \tag{11}$$

and where $\dot{\mathbf{u}} = \mathbf{v}$ denotes the velocity.

Substituting equation (10) into (7) and using (11) yields

$$\int_V \boldsymbol{\mathcal{C}} :: (\nabla_0 \delta \mathbf{u} \otimes \nabla_0 \mathbf{v}) \, dV = \int_{\partial V} \dot{\mathbf{t}}_0 \cdot \delta \mathbf{u} dA + \int_V \dot{\mathbf{f}}_0 \cdot \delta \mathbf{u} dV, \qquad \forall \delta \mathbf{u}, \tag{12}$$

and the equivalent indicial form,

$$\int_V \mathcal{C}_{ijkl} \frac{\partial \delta u_i}{\partial X_j} \frac{\partial v_k}{\partial X_l} dV = \int_{\partial V} \dot{t}_{0_i} \delta u_i dA + \int_V f_{0_i} \delta u_i dV. \tag{13}$$

This is the virtual work equation associated with hyperelasticity. The two-scale approach is described next. It is devised so that traditional FE continuum equations can be solved in the coarse scale and atomistic equations can be solved in the fine scale.

3. Homogenization

The homogenization framework enables the *weak* coupling of the continuum to the atoms. By taking the limit of the time-independent asymptotic expansion parameter $\varepsilon \to 0$, we

exploit the weak convergence properties of the scheme in order to decouple the length scales. At the fine scale, the domain contains only atoms with periodic conditions prescribed on the boundary, and all atom displacements are measured relative to a fixed point in the local frame of reference. From classical examples of continuum mechanics of composite materials [16], this enables the method to account for mutual interactions of periodically spaced heterogeneities or, in this case, periodic lattice defects.

The homogenization method is based on the assumption that two scales exist – a coarse scale and a fine scale. Coordinates in the coarse material scale are $\mathbf{X} = (X_1, X_2, X_3)$, and those in the fine material scale are $\mathbf{Y} = (Y_1, Y_2, Y_3)$. Likewise, the spatial coordinates are the lowercase analogues. The two scales are related by the scale parameter

$$\mathbf{Y} = \frac{\mathbf{X}}{\varepsilon}. \tag{14}$$

Therefore, we assume that the ratio of scales remains the same before and after deformation. The aim is to obtain two sets of coupled equations. The asymptotic series assumption decomposes the displacements as

$$\mathbf{u}(\mathbf{X}) = \mathbf{u}^{[0]}(\mathbf{X}) + \mathbf{u}^{[1]}(\mathbf{X}) \tag{15}$$

$$= \mathbf{u}^{[0]}(\mathbf{X}) + \varepsilon \mathbf{u}^{[1]}(\mathbf{Y}), \tag{16}$$

where $\mathbf{u}^{[0]}$ represents the displacement at the coarse scale and $\mathbf{u}^{[1]}$ represents the perturbed displacements due to inhomogeneity at the fine scale. Square brackets denote the order of the term in the asymptotic series. The actual physical representation of the total displacement at the fine scale is given by Takano et al. [17] as

$$\begin{aligned} \frac{1}{\varepsilon}\mathbf{u}(\mathbf{X}) &= \mathbf{u}^{\text{micro}}(\mathbf{Y}) \\ &= \mathbf{F}(\mathbf{u}^{[0]}(\mathbf{X}))\mathbf{Y} + \mathbf{u}^{[1]}(\mathbf{Y}). \end{aligned} \tag{17}$$

The variable $\mathbf{X}$ in equation (17) is a fixed value with respect to $\mathbf{Y}$. That is, the deformation gradient of a point in the coarse scale gets mapped onto a fine scale grid. This point is typically a quadrature point in an FE sense.

The time derivatives are analogous to equations (16) and (17). They are given as

$$\begin{aligned} \dot{\mathbf{u}}(\mathbf{X}) &= \mathbf{v}(\mathbf{X}) \\ &= \mathbf{v}^{[0]}(\mathbf{X}) + \varepsilon \mathbf{v}^{[1]}(\mathbf{Y}), \end{aligned} \tag{18}$$

$$\begin{aligned} \dot{\mathbf{u}}^{\text{micro}}(\mathbf{Y}) &= \mathbf{v}^{\text{micro}}(\mathbf{X}) \\ &= \mathbf{F}(\mathbf{v}^{[0]}(\mathbf{X}))\mathbf{Y} + \mathbf{v}^{[1]}(\mathbf{Y}). \end{aligned} \tag{19}$$

Substituting equations (16) and (18) into (13) yields

$$\begin{aligned} \int_V \boldsymbol{\mathcal{C}} :: \left[\nabla_X \left(\boldsymbol{\delta}\mathbf{u}^{[0]}(\mathbf{X}) + \varepsilon \boldsymbol{\delta}\mathbf{u}^{[1]}(\mathbf{Y})\right) \otimes \nabla_X \left(\mathbf{v}^{[0]}(\mathbf{X}) + \varepsilon \mathbf{v}^{[1]}(\mathbf{Y})\right)\right] dV \\ = \int_{\partial V} \left(\boldsymbol{\delta}\mathbf{u}^{[0]}(\mathbf{X}) + \varepsilon \boldsymbol{\delta}\mathbf{u}^{[1]}(\mathbf{Y})\right) \cdot \dot{\mathbf{t}}_0 dA \\ + \int_V \left(\boldsymbol{\delta}\mathbf{u}^{[0]}(\mathbf{X}) + \varepsilon \boldsymbol{\delta}\mathbf{u}^{[1]}(\mathbf{Y})\right) \cdot \dot{\mathbf{f}}_0 dV, \qquad \forall \boldsymbol{\delta}\mathbf{u}^{[0]}, \boldsymbol{\delta}\mathbf{u}^{[1]}. \end{aligned} \tag{20}$$

Note that by use of the chain rule and equation (14),

$$\begin{aligned} \nabla_X \phi(\mathbf{X}, \mathbf{Y}) &= \nabla_X \phi + \frac{\partial \mathbf{Y}}{\partial \mathbf{X}} \nabla_Y \phi \\ &= \nabla_X \phi + \frac{1}{\varepsilon} \nabla_Y \phi. \end{aligned} \tag{21}$$

Therefore,

$$\nabla_X \left(\mathbf{u}^{[0]}(\mathbf{X}) + \varepsilon \mathbf{u}^{[1]}(\mathbf{Y})\right) = \nabla_X \mathbf{u}^{[0]}(\mathbf{X}) + \nabla_Y \mathbf{u}^{[1]}(\mathbf{Y}). \tag{22}$$

Using equation (22) in (20) and taking the average over Y gives

$$\begin{aligned} \int_V \frac{1}{|Y|} \int_Y \boldsymbol{\mathcal{C}} :: \left[\left(\nabla_X \boldsymbol{\delta}\mathbf{u}^{[0]}(\mathbf{X}) + \nabla_Y \boldsymbol{\delta}\mathbf{u}^{[1]}(\mathbf{Y})\right) \otimes \left(\nabla_X \mathbf{v}^{[0]}(\mathbf{X}) + \nabla_Y \mathbf{v}^{[1]}(\mathbf{Y})\right)\right] dY dV \\ = \int_{\partial V} \left(\boldsymbol{\delta}\mathbf{u}^{[0]}(\mathbf{X}) + \varepsilon \boldsymbol{\delta}\mathbf{u}^{[1]}(\mathbf{Y})\right) \cdot \dot{\mathbf{t}}_0 dA \\ + \int_V \left(\boldsymbol{\delta}\mathbf{u}^{[0]}(\mathbf{X}) + \varepsilon \boldsymbol{\delta}\mathbf{u}^{[1]}(\mathbf{Y})\right) \cdot \dot{\mathbf{f}}_0 dV, \qquad \forall \boldsymbol{\delta}\mathbf{u}^{[0]}, \boldsymbol{\delta}\mathbf{u}^{[1]}. \end{aligned} \tag{23}$$

Then, in the limit as $\varepsilon \to 0$, equation (23) is satisfied only if the following two equations are satisfied,

$$\begin{aligned} \frac{1}{|Y|} \int_V \int_Y \boldsymbol{\mathcal{C}} :: \left[\nabla_X \boldsymbol{\delta}\mathbf{u}^{[0]}(\mathbf{X}) \otimes \left(\nabla_X \mathbf{v}^{[0]}(\mathbf{X}) + \nabla_Y \mathbf{v}^{[1]}(\mathbf{Y})\right)\right] dY dV \\ = \int_{\partial V} \boldsymbol{\delta}\mathbf{u}^{[0]}(\mathbf{X}) \cdot \dot{\mathbf{t}}_0 dA + \int_V \boldsymbol{\delta}\mathbf{u}^{[0]}(\mathbf{X}) \cdot \dot{\mathbf{f}}_0 dV, \qquad \forall\ \boldsymbol{\delta}\mathbf{u}^{[0]}, \end{aligned} \tag{24}$$

$$\frac{1}{|Y|}\int_V\int_Y \boldsymbol{\mathcal{C}} :: \left[\nabla_Y \delta\mathbf{u}^{[1]}(\mathbf{Y}) \otimes \left(\nabla_X \mathbf{v}^{[0]}(\mathbf{X}) + \nabla_Y \mathbf{v}^{[1]}(\mathbf{Y})\right)\right] dY dV = 0, \qquad \forall\ \delta\mathbf{u}^{[1]}. \tag{25}$$

By recourse to the FE method, the solution of equation (24) is straightforward, assuming $\boldsymbol{\mathcal{C}}$ and $\mathbf{v}^{[1]}$ are known. It is then evident that due to the dependence of equation (25) on $\mathbf{v}^{[0]}$, equations (24) and (25) are coupled and must be solved concurrently. For general problems, an iterative numerical solution scheme can be employed to handle the non-linear system of equations together with a linearly ramped load to ensure solution convergence.

In the next section, a method is shown for solving equation (25) for $\mathbf{v}^{[1]}$. Then in the following section, the formulation that enables the atomistic information to be fed into equation (24) is derived. These two sections constitute the iteration steps that must be performed for a general application.

4. Atomistic Equation

Distinct and distinguishable atoms are assumed to reside in the local level cell. By the Cauchy-Born rule [13], at a point $\mathbf{X}$, $\mathbf{F}(\mathbf{u}^{[0]})$ is assumed to give the energy minimizing configuration of the atoms. For simplicity, we assume that the atoms are arranged in a lattice.* Then, the positions of the atoms $\mathbf{Y}$ are given from the lattice coordinates $\mathbf{m}$ by

$$\mathbf{Y}_{(\mathbf{m})} = \mathbf{m}\mathbf{e}_i : \quad \mathbf{m} \in \mathcal{L}, \mathcal{L} = \mathbb{Z}^3, \mathbb{Z} \leq \mathbb{N}, \tag{26}$$

where $\mathbf{e}_i$ are the primitive translation vectors and $\mathbb{N}$ is the integer multiple of atoms contained in the unit cell. To avoid confusion in notation, atom labels are noted in parentheses henceforth and are not subject to the conventional summation rules associated with indicial notation. The displacement of the atoms are

$$\mathbf{q}_{(\mathbf{m})} : \quad \mathbf{m} \in \mathcal{L}. \tag{27}$$

*Note that there is no restriction to perfect lattices. In fact, by using computers, arbitrary arrangements of atoms can be considered as long as the assumption of the Cauchy-Born rule still applies.

Upon deformation, the new positions of the atoms are given by

$$\mathbf{y_{(m)}} = \mathbf{Y_{(m)}} + \mathbf{q_{(m)}}. \tag{28}$$

The deformation gradient is defined by

$$\mathbf{F} = \frac{\partial \mathbf{y}}{\partial \mathbf{Y}}. \tag{29}$$

The vector separating two atoms, i and j, in the reference configuration is given by

$$\mathbf{R}_{(ij)} = \mathbf{Y}_{(j)} - \mathbf{Y}_{(i)}, \tag{30}$$

where $\mathbf{Y}_{(j)}$ denotes the position of atom j; and $\mathbf{Y}_{(i)}$, the position of atom i. The vector separating two atoms in the deformed configuration is given by

$$\mathbf{r}_{(ij)} = \mathbf{y}_{(j)} - \mathbf{y}_{(i)}. \tag{31}$$

Then, the Cauchy-Born rule can be stated in a more precise manner by

$$\begin{aligned} \mathbf{r}_{(ij)} &= \mathbf{F}\mathbf{Y}_{(j)} - \mathbf{F}\mathbf{Y}_{(i)} \\ &= \mathbf{F}\mathbf{R}_{(ij)}. \end{aligned} \tag{32}$$

In defect regions and through the homogenization theory via equation (17), the rule becomes

$$\mathbf{r}_{(ij)} = \mathbf{F}\mathbf{R}_{(ij)} + \bar{\mathbf{r}}_{(ij)}, \tag{33}$$

where $\bar{\mathbf{r}}_{(ij)} = \mathbf{u}^{[1]}_{(j)} - \mathbf{u}^{[1]}_{(i)}$ is the additional term to account for high energy regions.

For the energy associated with the deformation of the atoms, we use a modified form of the so-called Potential II parameterization of the Tersoff-Brenner potential [18,19]. It takes the form

$$\mathcal{W} = \frac{1}{N}\left[E_b(\mathbf{Y}+\mathbf{q}) - E_b(\mathbf{Y})\right], \tag{34}$$

where $\mathcal{W}$ is the energy density of the frozen system, N is the number of atoms, and E_b is the binding energy given for a pure carbon system by

$$E_b(\mathbf{r}) = \sum_i \sum_{j(>i)} \left[V_R\left(r_{(ij)}\right) - \bar{B} V_A\left(r_{(ij)}\right) \right], \tag{35}$$

$$\bar{B} = \frac{1}{2}\left(B_{(ij)} + B_{(ji)}\right), \tag{36}$$

$$V_R(r) = \frac{f_{(ij)}(r) D^{(e)}}{(S-1)} e^{-\sqrt{2S}\beta(r-R^{(e)})}, \tag{37}$$

$$V_A(r) = \frac{f_{(ij)}(r) D^{(e)} S}{(S-1)} e^{-\sqrt{\frac{2}{S}}\beta(r-R^{(e)})}, \tag{38}$$

$$f_{(ij)}(r) = \begin{cases} 1, & r < R^{(1)} \\ \frac{1}{2}\left\{1 + \cos\left[\frac{\pi(r-R^{(1)})}{(r-R^{(2)})}\right]\right\}, & R^{(1)} < r < R^{(2)} \\ 0, & r > R^{(2)} \end{cases}, \tag{39}$$

$$B_{(ij)} = \left[1 + \sum_{k(\neq i,j)} G(\theta_{(ijk)}) f_{(ik)}\left(r_{(ik)}\right) \right]^{-\delta}, \tag{40}$$

$$G(\theta) = a_o \left\{ 1 + \frac{c_o^2}{d_o^2} - \frac{c_o^2}{d_o^2 + (1+\cos\theta)^2} \right\}, \tag{41}$$

with the constants given in Table 1. The modification in this work comes by way of omitting the extra bond-order term in [19], which is primarily used for problems involving changes in coordination numbers. We therefore presently restrict our consideration to classes of deformation involving no change in coordination.

Given that the energy can be written as a function of the atom displacements, equation (25) can be expressed in a form conducive to atom representations. We equate $\mathbf{v}^{[1]}$ to the rate of atom displacement and attempt to solve the equivalent form

$$\frac{\partial}{\partial Y_j} \mathcal{C}_{ijkl} \frac{\partial v_k^{[1]}}{\partial Y_l} = -\frac{\partial \mathcal{C}_{ijkl}}{\partial Y_j} \frac{\partial v_k^{[0]}}{\partial X_l} \tag{42}$$

under periodic boundary conditions. The solution to equation (42) is found as the zero of $\partial\mathcal{R}$ in the equation

$$\partial\boldsymbol{\mathcal{R}} = \boldsymbol{\mathcal{K}}\mathbf{v}^{[1]} - \boldsymbol{\mathcal{D}} \cdot \nabla_0 \mathbf{v}^{[0]}(\mathbf{x}), \tag{43}$$

Table 1. Parameters for Tersoff-Brenner potential.

$R^{(e)}$	1.39 Å
$D^{(e)}$	6.0 eV
S	1.22
β	2.1 Å
δ	0.5
$R^{(1)}$	1.7 Å
$R^{(2)}$	2.0 Å
a_o	0.00020813
c_o^2	330^2
d_o^2	3.5^2

where $\boldsymbol{\mathcal{K}}$ is the $N \times N$ Hessian and is given by

$$\boldsymbol{\mathcal{K}} = \frac{\partial^2 \mathcal{W}}{\partial \mathbf{q} \partial \mathbf{q}}, \tag{44}$$

where $\mathbf{q}$ is the vector of atom displacements of size $3N$ (in three dimensions) and $\boldsymbol{\mathcal{D}}$ is a third-order unsymmetric tensor that is obtained from the first derivative of the Euler-Lagrange equation with respect to the local deformation gradient given by

$$\boldsymbol{\mathcal{D}} = -\frac{\partial^2 \mathcal{W}}{\partial \mathbf{q} \partial \mathbf{F}}. \tag{45}$$

The size of $\boldsymbol{\mathcal{D}}$ depends on the dimensionality of the problem. In three dimensions, it can be expressed as an $N \times 9$ matrix, where 9 corresponds to the number of independent components of $\mathbf{F}$.

5. Multiscale Equation

Once equation (43) has been solved for $\mathbf{v}^{[1]}$, the remaining task is to formulate a tractable global scale boundary value problem. The key distinction between this investigation and

conventional continuum formulations, such as hyperelasticity, is the conspicuous incorporation of $\mathbf{v}^{[1]}$, a fine-scale/atomistic quantity, in the global scale equations, and the definition of the material property tensor completely in terms of atomistic variables.

We return to equation (24), recognizing that $\mathbf{v}^{[1]}$ is now known. Incorporating the definition for the first Lagrangian elasticity tensor from equation (9) yields

$$\begin{aligned}\frac{1}{|Y|}\int_V\int_Y \frac{\partial^2 \mathcal{W}}{\partial \mathbf{F}\partial \mathbf{F}} :: \left[\nabla_X \boldsymbol{\delta}\mathbf{u}^{[0]}(\mathbf{X}) \otimes \left(\nabla_X \mathbf{v}^{[0]}(\mathbf{X}) + \nabla_Y \mathbf{v}^{[1]}(\mathbf{Y})\right)\right] dY dV \\ = \int_{\partial V} \boldsymbol{\delta}\mathbf{u}^{[0]}(\mathbf{X}) \cdot \dot{\mathbf{t}}_0 dA + \int_V \boldsymbol{\delta}\mathbf{u}^{[0]}(\mathbf{X}) \cdot \dot{\mathbf{f}}_0 dV, \qquad \forall\ \boldsymbol{\delta}\mathbf{u}^{[0]}.\end{aligned} \tag{46}$$

Then, using the definition of $\mathbf{F}$ in equation (1) and assuming a first-order Taylor series representation for the time derivative gives,

$$\begin{aligned}\frac{1}{|Y|}\int_V\int_Y \frac{\partial^2 \mathcal{W}}{\partial \mathbf{F}\partial \mathbf{F}} :: \left(\nabla_X \boldsymbol{\delta}\mathbf{u}^{[0]}(\mathbf{X}) \otimes \nabla_X \mathbf{v}^{[0]}(\mathbf{X})\right) dY dV \\ = \int_{\partial V} \boldsymbol{\delta}\mathbf{u}^{[0]}(\mathbf{X}) \cdot \dot{\mathbf{t}}_0 dA + \int_V \boldsymbol{\delta}\mathbf{u}^{[0]}(\mathbf{X}) \cdot \dot{\mathbf{f}}_0 dV \\ - \frac{1}{|Y|}\int_V\int_Y \frac{\partial^2 \mathcal{W}}{\partial \mathbf{F}\partial \mathbf{q}} :\cdot \left(\nabla_X \boldsymbol{\delta}\mathbf{u}^{[0]}(\mathbf{X}) \otimes \mathbf{v}^{[1]}(\mathbf{Y})\right) dY dV, \qquad \forall\ \boldsymbol{\delta}\mathbf{u}^{[0]},\end{aligned} \tag{47}$$

where there is now a double contraction on $\nabla_X \boldsymbol{\delta u}^{[0]}$ and a single contraction on $\mathbf{v}^{[1]}$ in the last expression of equation (47). The solution to equation (47) yields $\mathbf{v}^{[0]}$. It is noteworthy that the last term is zero when the energy distribution over Y is constant, i.e., when the atom arrangement forms a perfect lattice. This reduces the problem to a classical harmonic approximation where the first Lagrangian elasticity tensor is assumed to model the material behavior. In equation (47), the last term serves as a corrective force in regions of highly energetic atoms (i.e., nonlocal regions) to account for defects and lattice inhomogeneities.

6. The Euler-Lagrange Equations and the Hessian

In this section, the analytic forms of the Euler-Lagrange equations and Hessian are derived for a general potential. The nontrivial algebra typically needed to obtain equations (44) and

(45) for the specific case of the Tersoff-Brenner potential are shown in greater detail in [14], and only general forms are derived here. The Euler-Lagrange equation is the first derivative of the Lagrangian with respect to the degrees of freedom. In this problem, the Lagrangian is the negative of the atomistic energy density, which we presently assume is equivalent to the free energy at zero temperature. The Euler-Lagrange equation is therefore given by

$$\begin{aligned} \mathcal{E} &= \frac{\partial \mathcal{W}}{\partial \mathbf{q}_{(m)}} \\ &= \frac{1}{N}\frac{\partial E_b}{\partial \mathbf{q}_{(m)}}, \end{aligned} \tag{48}$$

and using the chain rule for derivatives, it is

$$\begin{aligned} \mathcal{E} &= \frac{1}{N}\frac{\partial E_b}{\partial \mathbf{q}_{(m)}} \\ &= \frac{1}{N}\left(\frac{\partial E_b}{\partial \mathbf{r}_{(ij)}}\cdot\frac{\partial \mathbf{r}_{(ij)}}{\partial \mathbf{q}_{(m)}} + \frac{\partial E_b}{\partial \mathbf{r}_{(ik)}}\cdot\frac{\partial \mathbf{r}_{(ik)}}{\partial \mathbf{q}_{(m)}} + \frac{\partial E_b}{\partial \mathbf{r}_{(jk)}}\cdot\frac{\partial \mathbf{r}_{(jk)}}{\partial \mathbf{q}_{(m)}}\right). \end{aligned} \tag{49}$$

Here, we have implicitly assumed that there are three independent atomic position vectors. One can show quite easily that there are in fact only two by using the relationship $\mathbf{r}_{(jk)} = \mathbf{r}_{(ik)} - \mathbf{r}_{(ij)}$.

The Hessian is obtained by taking an additional derivative of the Euler-Lagrange equations. Specifically, we again make use of the chain rule to obtain

$$\begin{aligned} \mathcal{K} &= \frac{\partial^2 \mathcal{W}}{\partial \mathbf{q}_{(n)}\partial \mathbf{q}_{(m)}} \\ &= \frac{1}{N}\frac{\partial^2 E_b}{\partial \mathbf{q}_{(n)}\partial \mathbf{q}_{(m)}} \\ &= \frac{1}{N}\left[\frac{\partial^2 E_b}{\partial \mathbf{r}_{(ij)}\partial \mathbf{r}_{(ij)}} : \left(\frac{\partial \mathbf{r}_{(ij)}}{\partial \mathbf{q}_{(n)}}\otimes\frac{\partial \mathbf{r}_{(ij)}}{\partial \mathbf{q}_{(m)}}\right) + \frac{\partial^2 E_b}{\partial \mathbf{r}_{(ij)}\partial \mathbf{r}_{(ik)}} : \left(\frac{\partial \mathbf{r}_{(ij)}}{\partial \mathbf{q}_{(n)}}\otimes\frac{\partial \mathbf{r}_{(ik)}}{\partial \mathbf{q}_{(m)}}\right)\right. \\ &\quad + \frac{\partial^2 E_b}{\partial \mathbf{r}_{(ik)}\partial \mathbf{r}_{(ij)}} : \left(\frac{\partial \mathbf{r}_{(ik)}}{\partial \mathbf{q}_{(n)}}\otimes\frac{\partial \mathbf{r}_{(ij)}}{\partial \mathbf{q}_{(m)}}\right) + \frac{\partial^2 E_b}{\partial \mathbf{r}_{(ik)}\partial \mathbf{r}_{(ik)}} : \left(\frac{\partial \mathbf{r}_{(ik)}}{\partial \mathbf{q}_{(n)}}\otimes\frac{\partial \mathbf{r}_{(ik)}}{\partial \mathbf{q}_{(m)}}\right) \\ &\quad + \frac{\partial^2 E_b}{\partial \mathbf{r}_{(jk)}\partial \mathbf{r}_{(jk)}} : \left(\frac{\partial \mathbf{r}_{(jk)}}{\partial \mathbf{q}_{(n)}}\otimes\frac{\partial \mathbf{r}_{(jk)}}{\partial \mathbf{q}_{(m)}}\right) + \frac{\partial^2 E_b}{\partial \mathbf{r}_{(ij)}\partial \mathbf{r}_{(jk)}} : \left(\frac{\partial \mathbf{r}_{(ij)}}{\partial \mathbf{q}_{(n)}}\otimes\frac{\partial \mathbf{r}_{(jk)}}{\partial \mathbf{q}_{(m)}}\right) \\ &\quad + \frac{\partial^2 E_b}{\partial \mathbf{r}_{(jk)}\partial \mathbf{r}_{(ij)}} : \left(\frac{\partial \mathbf{r}_{(jk)}}{\partial \mathbf{q}_{(n)}}\otimes\frac{\partial \mathbf{r}_{(ij)}}{\partial \mathbf{q}_{(m)}}\right) + \frac{\partial^2 E_b}{\partial \mathbf{r}_{(ik)}\partial \mathbf{r}_{(jk)}} : \left(\frac{\partial \mathbf{r}_{(ik)}}{\partial \mathbf{q}_{(n)}}\otimes\frac{\partial \mathbf{r}_{(jk)}}{\partial \mathbf{q}_{(m)}}\right) \\ &\quad \left. + \frac{\partial^2 E_b}{\partial \mathbf{r}_{(jk)}\partial \mathbf{r}_{(ik)}} : \left(\frac{\partial \mathbf{r}_{(jk)}}{\partial \mathbf{q}_{(n)}}\otimes\frac{\partial \mathbf{r}_{(ik)}}{\partial \mathbf{q}_{(m)}}\right)\right]. \end{aligned} \tag{50}$$

Second derivatives of the interatom vectors are zero, i.e.,

$$\frac{\partial^2 \mathbf{r}_{(ij)}}{\partial \mathbf{q}_{(m)} \partial \mathbf{q}_{(n)}} = \frac{\partial^2}{\partial \mathbf{q}_{(m)} \partial \mathbf{q}_{(n)}} \left(\mathbf{Y}_{(j)} + \mathbf{q}_{(j)} - \mathbf{Y}_{(i)} + \mathbf{q}_{(i)} \right) \tag{51}$$

$$= \mathbf{0} \qquad \forall (m, n). \tag{52}$$

Next, the appropriate right-hand side expressions are derived for equations (43) and (45). This involves the use of the chain rule again to obtain

$$\begin{aligned} \frac{\partial^2 \mathcal{W}}{\partial \mathbf{q}_{(m)} \partial \mathbf{F}} = \frac{1}{N} \Bigg[& \frac{\partial^2 E_b}{\partial \mathbf{r}_{(ij)} \partial \mathbf{r}_{(ij)}} : \left(\frac{\partial \mathbf{r}_{(ij)}}{\partial \mathbf{F}} \otimes \frac{\partial \mathbf{r}_{(ij)}}{\partial \mathbf{q}_{(m)}} \right) + \frac{\partial^2 E_b}{\partial \mathbf{r}_{(ij)} \partial \mathbf{r}_{(ik)}} : \left(\frac{\partial \mathbf{r}_{(ik)}}{\partial \mathbf{F}} \otimes \frac{\partial \mathbf{r}_{(ij)}}{\partial \mathbf{q}_{(m)}} \right) \\ & + \frac{\partial^2 E_b}{\partial \mathbf{r}_{(ik)} \partial \mathbf{r}_{(ij)}} : \left(\frac{\partial \mathbf{r}_{(ij)}}{\partial \mathbf{F}} \otimes \frac{\partial \mathbf{r}_{(ik)}}{\partial \mathbf{q}_{(m)}} \right) + \frac{\partial^2 E_b}{\partial \mathbf{r}_{(ik)} \partial \mathbf{r}_{(ik)}} : \left(\frac{\partial \mathbf{r}_{(ik)}}{\partial \mathbf{F}} \otimes \frac{\partial \mathbf{r}_{(ik)}}{\partial \mathbf{q}_{(m)}} \right) \\ & + \frac{\partial^2 E_b}{\partial \mathbf{r}_{(ij)} \partial \mathbf{r}_{(jk)}} : \left(\frac{\partial \mathbf{r}_{(jk)}}{\partial \mathbf{F}} \otimes \frac{\partial \mathbf{r}_{(ij)}}{\partial \mathbf{q}_{(m)}} \right) + \frac{\partial^2 E_b}{\partial \mathbf{r}_{(jk)} \partial \mathbf{r}_{(ij)}} : \left(\frac{\partial \mathbf{r}_{(ij)}}{\partial \mathbf{F}} \otimes \frac{\partial \mathbf{r}_{(jk)}}{\partial \mathbf{q}_{(m)}} \right) \\ & + \frac{\partial^2 E_b}{\partial \mathbf{r}_{(ik)} \partial \mathbf{r}_{(jk)}} : \left(\frac{\partial \mathbf{r}_{(jk)}}{\partial \mathbf{F}} \otimes \frac{\partial \mathbf{r}_{(ik)}}{\partial \mathbf{q}_{(m)}} \right) + \frac{\partial^2 E_b}{\partial \mathbf{r}_{(jk)} \partial \mathbf{r}_{(ik)}} : \left(\frac{\partial \mathbf{r}_{(ik)}}{\partial \mathbf{F}} \otimes \frac{\partial \mathbf{r}_{(jk)}}{\partial \mathbf{q}_{(m)}} \right) \\ & + \frac{\partial^2 E_b}{\partial \mathbf{r}_{(jk)} \partial \mathbf{r}_{(jk)}} : \left(\frac{\partial \mathbf{r}_{(jk)}}{\partial \mathbf{F}} \otimes \frac{\partial \mathbf{r}_{(jk)}}{\partial \mathbf{q}_{(m)}} \right) \Bigg], \end{aligned} \tag{53}$$

and by definition,

$$\frac{\partial \mathbf{r}_{(ij)}}{\partial \mathbf{F}} = \mathbf{R}_{(ij)} \qquad \text{and} \qquad \frac{\partial \mathbf{r}_{(ik)}}{\partial \mathbf{F}} = \mathbf{R}_{(ik)}. \tag{54}$$

Finally, we use a similar approach to define the first Lagrangian elasticity tensor. This is the traditional way of estimating the elastic properties of a solid. Using the chain rule once again gives

$$\begin{aligned} \frac{\partial^2 \mathcal{W}}{\partial \mathbf{F} \partial \mathbf{F}} = \frac{1}{N} \Bigg[& \frac{\partial^2 E_b}{\partial \mathbf{r}_{(ij)} \partial \mathbf{r}_{(ij)}} : \left(\frac{\partial \mathbf{r}_{(ij)}}{\partial \mathbf{F}} \otimes \frac{\partial \mathbf{r}_{(ij)}}{\partial \mathbf{F}} \right) + \frac{\partial^2 E_b}{\partial \mathbf{r}_{(ij)} \partial \mathbf{r}_{(ik)}} : \left(\frac{\partial \mathbf{r}_{(ik)}}{\partial \mathbf{F}} \otimes \frac{\partial \mathbf{r}_{(ij)}}{\partial \mathbf{F}} \right) \\ & + \frac{\partial^2 E_b}{\partial \mathbf{r}_{(ik)} \partial \mathbf{r}_{(ij)}} : \left(\frac{\partial \mathbf{r}_{(ij)}}{\partial \mathbf{F}} \otimes \frac{\partial \mathbf{r}_{(ik)}}{\partial \mathbf{F}} \right) + \frac{\partial^2 E_b}{\partial \mathbf{r}_{(ik)} \partial \mathbf{r}_{(ik)}} : \left(\frac{\partial \mathbf{r}_{(ik)}}{\partial \mathbf{F}} \otimes \frac{\partial \mathbf{r}_{(ik)}}{\partial \mathbf{F}} \right) \\ & + \frac{\partial^2 E_b}{\partial \mathbf{r}_{(ij)} \partial \mathbf{r}_{(jk)}} : \left(\frac{\partial \mathbf{r}_{(jk)}}{\partial \mathbf{F}} \otimes \frac{\partial \mathbf{r}_{(ij)}}{\partial \mathbf{F}} \right) + \frac{\partial^2 E_b}{\partial \mathbf{r}_{(jk)} \partial \mathbf{r}_{(ij)}} : \left(\frac{\partial \mathbf{r}_{(ij)}}{\partial \mathbf{F}} \otimes \frac{\partial \mathbf{r}_{(jk)}}{\partial \mathbf{F}} \right) \\ & + \frac{\partial^2 E_b}{\partial \mathbf{r}_{(ik)} \partial \mathbf{r}_{(jk)}} : \left(\frac{\partial \mathbf{r}_{(jk)}}{\partial \mathbf{F}} \otimes \frac{\partial \mathbf{r}_{(ik)}}{\partial \mathbf{F}} \right) + \frac{\partial^2 E_b}{\partial \mathbf{r}_{(jk)} \partial \mathbf{r}_{(ik)}} : \left(\frac{\partial \mathbf{r}_{(ik)}}{\partial \mathbf{F}} \otimes \frac{\partial \mathbf{r}_{(jk)}}{\partial \mathbf{F}} \right) \\ & + \frac{\partial^2 E_b}{\partial \mathbf{r}_{(jk)} \partial \mathbf{r}_{(jk)}} : \left(\frac{\partial \mathbf{r}_{(jk)}}{\partial \mathbf{F}} \otimes \frac{\partial \mathbf{r}_{(jk)}}{\partial \mathbf{F}} \right) \Bigg]. \end{aligned} \tag{55}$$

The first Lagrangian elasticity tensor is used in equation (47), whose solution gives $\mathbf{v}^{[0]}$. In a perfect lattice, equation (55) provides the only atomistic material information needed to solve the macroscopic continuum problem. The next section illustrates this by showing that the perturbation is zero for a uniform crystal.

7. Example Problems

7.1 Example I: Perfect 1-D Atomic Lattice

To illustrate the calculation, a 1-D analytical example is presented. The Tersoff-Brenner potential is used to represent the energetics of a 1-D single-species chain of carbon atoms. The objective here is to solve equations (42) and (43) for $v^{[1]}$ and demonstrate a simple case of a perfect lattice using this method.

One atom comprises the periodic unit cell, but to account for the effects of triples, two "fictitious" atoms are assumed to extend beyond the boundaries of the cell on each side as illustrated in Figure 3. Periodic conditions apply at the cell boundaries. The equilibrium lattice constant for the chain is $r_o = 1.86868\mathring{A}$.

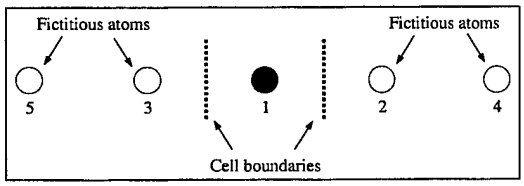

Figure 3. Unit cell of the 1-D carbon chain. The atoms are labeled by identifying numbers.

The following two conditions stem from the 1-D assumption,

$$\begin{aligned} &\theta = \pi, \\ &R^{(1)} < r < R^{(2)}. \end{aligned} \tag{56}$$

This simplifies the expressions in [14]. The resulting Hessian for three arbitrary colinear atoms (i, j, k) is obtained as

$$\left[\mathcal{K}^{(ijk)}\right] = \begin{bmatrix} \mathcal{K}_{11}^{(ijk)} & \mathcal{K}_{12}^{(ijk)} & \mathcal{K}_{13}^{(ijk)} \\ \mathcal{K}_{21}^{(ijk)} & \mathcal{K}_{22}^{(ijk)} & \mathcal{K}_{23}^{(ijk)} \\ \mathcal{K}_{31}^{(ijk)} & \mathcal{K}_{32}^{(ijk)} & \mathcal{K}_{33}^{(ijk)} \end{bmatrix}, \tag{57}$$

where $\mathcal{K}_{mn}^{(ijk)} = \mathcal{K}_{nm}^{(ijk)}$ and the terms are defined by

$$\begin{aligned} \mathcal{K}_{11}^{(ijk)} &= V_R'' - \bar{B}V_A'' + a_o\delta V_A' B_{(ij)}^{1+\frac{1}{\delta}} f_{(ik)}' + \frac{\delta}{2}(\delta+1)V_A B_{(ij)}^{1+\frac{2}{\delta}} \left(a_o f_{(ik)}'\right)^2 \\ &\quad + \frac{a_o\delta}{2} V_A B_{(ij)}^{1+\frac{1}{\delta}} f_{(ik)}'', \end{aligned} \tag{58}$$

$$\mathcal{K}_{12}^{(ijk)} = -V_R'' + \bar{B}V_A'' - \frac{a_o\delta}{2} V_A' B_{(ij)}^{1+\frac{1}{\delta}} f_{(ik)}', \tag{59}$$

$$\mathcal{K}_{13}^{(ijk)} = -\frac{a_o\delta}{2} V_A' B_{(ij)}^{1+\frac{1}{\delta}} f_{(ik)}' - \frac{\delta}{2}(\delta+1)V_A B_{(ij)}^{1+\frac{2}{\delta}} \left(a_o f_{(ik)}'\right)^2 - \frac{a_o\delta}{2} V_A B_{(ij)}^{1+\frac{1}{\delta}} f_{(ik)}'', \tag{60}$$

$$\mathcal{K}_{22}^{(ijk)} = V_R'' - \bar{B}V_A'', \tag{61}$$

$$\mathcal{K}_{23}^{(ijk)} = \frac{a_o\delta}{2} V_A' B_{(ij)}^{1+\frac{1}{\delta}} f_{(ik)}', \tag{62}$$

$$\mathcal{K}_{33}^{(ijk)} = \frac{\delta}{2}(\delta+1)V_A B_{(ij)}^{1+\frac{2}{\delta}} \left(a_o f_{(ik)}'\right)^2 + \frac{a_o\delta}{2} V_A B_{(ij)}^{1+\frac{1}{\delta}} f_{(ik)}''. \tag{63}$$

Upon assembly of the two unique pairs (31,12) and their associated triples (123,132) in Figure 3, the final assembled Hessian of the global system is given by the matrix,

$$[\mathcal{K}] = \begin{bmatrix} \mathcal{K}_{11} & \mathcal{K}_{12} & \mathcal{K}_{13} \\ \mathcal{K}_{21} & \mathcal{K}_{22} & \mathcal{K}_{23} \\ \mathcal{K}_{31} & \mathcal{K}_{32} & \mathcal{K}_{33} \end{bmatrix}, \tag{64}$$

which is assembled through the operation,

$$[\mathcal{K}] = \bigsqcup_{(m)}^{(i,j,k)} \bigsqcup_{(n)}^{(i,j,k)} \left[\mathcal{K}^{(ijk)}\right] = \mathcal{K}_{mn}, \tag{65}$$

where $\bigsqcup$ is the addition operator over all unique pair and triple combinations of (i,j,k) and (m) and (n) are displacement degrees of freedom for each atom. In equation (65), $[\mathcal{K}]$ is symmetric once again, and its components are obtained in detail for the problem shown in Figure 3 as follows:

$$\mathcal{K}_{11} = \mathcal{K}_{11}^{(123)} + \mathcal{K}_{22}^{(315)} + \mathcal{K}_{33}^{(241)}, \tag{66}$$

$$\mathcal{K}_{12} = \mathcal{K}_{12}^{(123)} + \mathcal{K}_{13}^{(241)}, \tag{67}$$

$$\mathcal{K}_{13} = \mathcal{K}_{13}^{(123)} + \mathcal{K}_{12}^{(315)}, \tag{68}$$

$$\mathcal{K}_{22} = \mathcal{K}_{22}^{(123)} + \mathcal{K}_{11}^{(241)}, \tag{69}$$

$$\mathcal{K}_{23} = \mathcal{K}_{23}^{(123)}, \tag{70}$$

$$\mathcal{K}_{33} = \mathcal{K}_{33}^{(123)} + \mathcal{K}_{11}^{(315)}. \tag{71}$$

This constitutes the stiffness matrix $\boldsymbol{\mathcal{K}}$ in equation (43).

The next step is to calculate the right-hand side of equation (42), which is equivalent to calculating $\boldsymbol{\mathcal{D}}$ and multiplying by the global rate of the deformation gradient. Using equations (45) and (53), the right-hand side for three colinear atoms (i,j,k) is obtained as

$$\left\{\mathcal{D}^{(ijk)}\right\} = \left\{ \begin{array}{c} \mathcal{D}_1^{(ijk)} \\ \mathcal{D}_2^{(ijk)} \\ \mathcal{D}_3^{(ijk)} \end{array} \right\}, \tag{72}$$

where the components are defined by

$$\begin{aligned} \mathcal{D}_1^{(ijk)} =& R_{(ij)} \left(V_R'' - \bar{B} V_A'' \right) + \left(R_{(ik)} - R_{(ij)} \right) \left(\frac{a_o \delta}{2} V_A' B_{(ij)}^{1+\frac{1}{\delta}} f_{(ik)}' \right) \\ &+ R_{(ik)} \left(\frac{\delta}{2} (\delta+1) V_A B_{(ij)}^{1+\frac{2}{\delta}} \left(a_o f_{(ik)}' \right)^2 + \frac{a_o \delta}{2} V_A B_{(ij)}^{1+\frac{1}{\delta}} f_{(ik)}'' \right), \end{aligned} \tag{73}$$

$$\mathcal{D}_2^{(ijk)} = - R_{(ij)} \left(V_R'' - \bar{B} V_A'' \right) - R_{(ik)} \left(\frac{a_o \delta}{2} V_A' B_{(ij)}^{1+\frac{1}{\delta}} f_{(ik)}' \right), \tag{74}$$

$$\begin{aligned} \mathcal{D}_3^{(ijk)} =& - R_{(ij)} \left(\frac{a_o \delta}{2} V_A' B_{(ij)}^{1+\frac{1}{\delta}} f_{(ik)}' \right) \\ &- R_{(ik)} \left(\frac{\delta}{2} (\delta+1) V_A B_{(ij)}^{1+\frac{2}{\delta}} \left(a_o f_{(ik)}' \right)^2 + \frac{a_o \delta}{2} V_A B_{(ij)}^{1+\frac{1}{\delta}} f_{(ik)}'' \right). \end{aligned} \tag{75}$$

As earlier, the assembly operation

$$\{\mathcal{D}\} = \bigsqcup_{(m)}^{(i,j,k)} \{\mathcal{D}^{(ijk)}\} = \mathcal{D}_m, \tag{76}$$

yields the right-hand side of the global system given by,

$$\{\mathcal{D}\} = \begin{Bmatrix} \mathcal{D}_1 \\ \mathcal{D}_2 \\ \mathcal{D}_3 \end{Bmatrix}, \tag{77}$$

where the components are

$$\mathcal{D}_1 = \mathcal{D}_1^{(123)} + \mathcal{D}_2^{(315)} + \mathcal{D}_3^{(241)}, \tag{78}$$

$$\mathcal{D}_2 = \mathcal{D}_2^{(123)} + \mathcal{D}_1^{(241)}, \tag{79}$$

$$\mathcal{D}_3 = \mathcal{D}_3^{(123)} + \mathcal{D}_1^{(315)}. \tag{80}$$

Under the assumption of a 1-D perfect lattice, we have $R_{(ij)} = R_{(ik)}$ and, consequently, $\mathcal{D}_1 = 0$. Then, we can satisfy the periodicity condition and the rigid body constraint by setting $v_{(2)}^{[1]} = v_{(3)}^{[1]} = 0$. The solution is therefore

$$v_{(1)}^{[1]} = v_{(2)}^{[1]} = v_{(3)}^{[1]} = 0. \tag{81}$$

In light of equation (81), the last term in equation (47) is zero, and the material properties are obtained from the atomistic energy density solely through equation (55). This result shows that in a defect-free lattice, the homogenization method coincides with the conventional atomistic hyperelasticity problem. The next section shows an example in which a defect causes an inhomogeneous energy distribution, leading to a situation where homogenization is needed to average out the energy.

7.2 Example II: 1-D Atomic Lattice With Defect

Consider the problem shown in Figure 4, where the center atom is displaced by a distance L from its original energy minimizing configuration. This displacement of the center atom

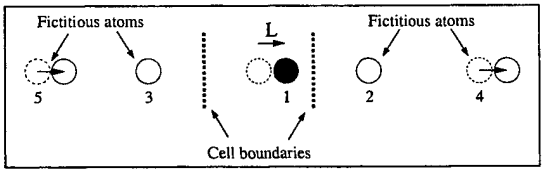

Figure 4. Unit cell of one-dimensional carbon chain with periodic defect.

constitutes the defect.

With this change, the key stiffness matrix term in equation (66) is now

$$\begin{aligned}\mathcal{K}_{11} =& V''_{R_{(12)}} - \bar{B}_{(12)} V''_{A_{(12)}} + a_o \delta V'_{A_{(12)}} B_{(12)}^{1+\frac{1}{\delta}} f'_{(13)} \\ &+ \frac{\delta}{2}(\delta+1) V_{A_{(12)}} B_{(12)}^{1+\frac{2}{\delta}} \left(a_o f'_{(13)}\right)^2 + \frac{a_o \delta}{2} V_{A_{(12)}} B_{(12)}^{1+\frac{1}{\delta}} f''_{(13)} \\ &+ V''_{R_{(13)}} - \bar{B}_{(13)} V''_{A_{(13)}} + a_o \delta V'_{A_{(13)}} B_{(13)}^{1+\frac{1}{\delta}} f'_{(12)} \\ &+ \frac{\delta}{2}(\delta+1) V_{A_{(13)}} B_{(13)}^{1+\frac{2}{\delta}} \left(a_o f'_{(12)}\right)^2 + \frac{a_o \delta}{2} V_{A_{(13)}} B_{(13)}^{1+\frac{1}{\delta}} f''_{(12)},\end{aligned} \tag{82}$$

and likewise, equation (78) is now

$$\begin{aligned}\mathcal{D}_1 =& R_{(12)} \left(V''_{R_{(12)}} - \bar{B}_{(12)} V''_{A_{(12)}}\right) + \left(R_{(13)} - R_{(12)}\right) \left(\frac{a_o \delta}{2} V'_{A_{(12)}} B_{(12)}^{1+\frac{1}{\delta}} f'_{(13)}\right) \\ &+ R_{(13)} \left(\frac{\delta}{2}(\delta+1) V_{A_{(12)}} B_{(12)}^{1+\frac{2}{\delta}} \left(a_o f'_{(13)}\right)^2 + \frac{a_o \delta}{2} V_{A_{(12)}} B_{(12)}^{1+\frac{1}{\delta}} f''_{(13)}\right) \\ &- R_{(13)} \left(V''_{R_{(13)}} - \bar{B}_{(13)} V''_{A_{(13)}}\right) - \left(R_{(12)} - R_{(13)}\right) \left(\frac{a_o \delta}{2} V'_{A_{(13)}} B_{(13)}^{1+\frac{1}{\delta}} f'_{(12)}\right) \\ &- R_{(12)} \left(\frac{\delta}{2}(\delta+1) V_{A_{(13)}} B_{(13)}^{1+\frac{2}{\delta}} \left(a_o f'_{(12)}\right)^2 + \frac{a_o \delta}{2} V_{A_{(13)}} B_{(13)}^{1+\frac{1}{\delta}} f''_{(12)}\right),\end{aligned} \tag{83}$$

where $R_{(12)} = r_o - L$ and $R_{(13)} = r_o + L$. Then, solving equation (43) under periodic boundary conditions gives

$$v_1^{[1]} = \frac{\mathcal{D}_1}{\mathcal{K}_1} \frac{\partial v^{[0]}}{\partial x}, \quad v_2^{[1]} = v_3^{[1]} = 0. \tag{84}$$

The $v^{[1]}/\nabla_0 v^{[0]}$ solution as a function of L/r_o is shown in Figure 5. As expected, the solution has symmetry about the origin and grows asymptotically larger as the size of the defect (L) grows closer to the cut-off radii. We intentionally avoid larger defects due to the nonconvex

structure of the energy well associated with the Tersoff-Brenner potential. This generally leads to unphysical discontinuities in the perturbation velocity ($v^{[1]}$) due to discontinuous second derivatives of the atomistic energy with respect to the defect size. This is attributable to the construction of the empirical potential in equations (35)–(41), which is suited, by design, for systems where nearest neighbor atoms, even in defect regions, are within the cut-off radius $R^{(2)}$.

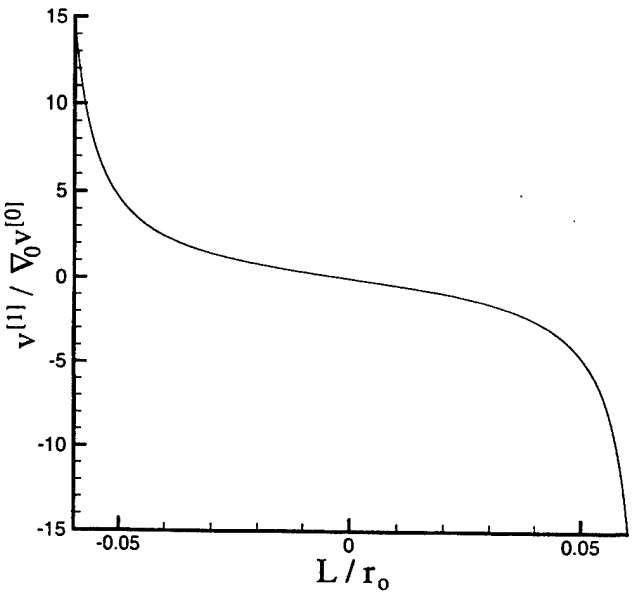

Figure 5. Distribution of $v^{[1]}/\nabla_0 v^{[0]}$ solution as a function of the defect size L.

It is also noteworthy that arbitrary defect densities can be treated by appropriate modification of the unit cell. In most cases, one can tailor the desired density by increasing the size of the unit cell and performing the summations and the assembly of the atomistic discrete equations over more atoms. Figure 6 illustrates this idea for the 1-D carbon chain.

Numerical experiments show that as the size of the unit cell increases, the perturbative

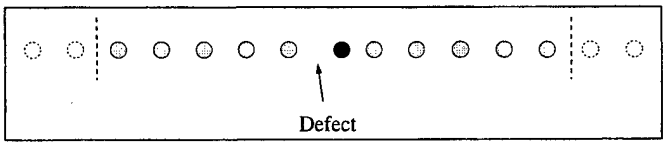

Figure 6. Larger chain of atoms in perfect arrangement around the defect region decreases the defect density.

displacement has a sharp discontinuity at the defect. Figure 7 shows this nonlocal behavior as the number of atoms increases. The problem is of a single defect in chains of increasing size. The defect magnitude is held fixed at $L/r_o = 0.01$. The nonlocal discontinuity of the perturbative velocity qualitatively agrees with traditional displacement jumps that occur at dislocation cores. The discontinuity indicates that the material property at the defect ($\frac{\partial^2 W}{\partial \mathbf{F} \partial \mathbf{F}}$) is modified by the last term in equation (47), an amount proportional to $v^{[1]}$ that serves as a correcting force for the nonlocal effect.

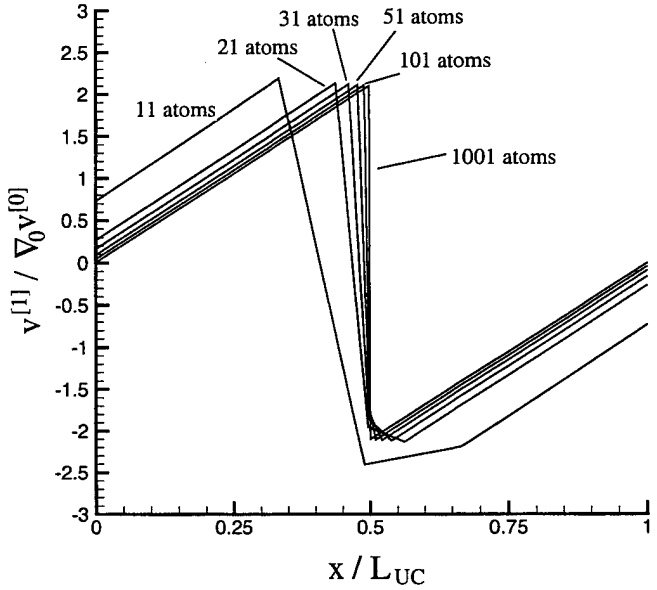

Figure 7. Distribution of $v^{[1]}/\nabla_0 v^{[0]}$ along unit cell length for varying numbers of atoms ($L/r_o = 0.01$).

Although the primary details of the method have been demonstrated in these two examples, the method can be extended to consider the multiscale problem shown in equation (47) for more general cases involving self-consistent solutions with equation (43) as in the next section.

7.3 Example III: 2-D Graphene With Defect

The method can be generalized to multiaxial problems. In this example, we consider graphene with three types of point defects: interstitial, equilibrium point vacancy and saddle point vacancy. The atom positions around the point defects were first computed using quenched molecular dynamics. These are illustrated in Figure 8 together with the original defect-free configuration. Similar defect structures have been encountered both numerically and experimentally [20–22].

The effective elastic constants for the defect-free case were in the form of the first Lagrangian elasticity tensor (55), which compare reasonably with experimental results. Using the second derivative of the Tersoff-Brenner potential, the bulk values (in units eV/atom) for graphene were computed,

$$\mathcal{C}_{1111} = 66.51 \quad \mathcal{C}_{2112} = 21.63, \tag{85}$$

$$\mathcal{C}_{1122} = 20.06 \quad \mathcal{C}_{2121} = 24.83, \tag{86}$$

$$\mathcal{C}_{1212} = 24.83 \quad \mathcal{C}_{2211} = 20.06, \tag{87}$$

$$\mathcal{C}_{1221} = 21.63 \quad \mathcal{C}_{2222} = 66.51, \tag{88}$$

and terms not listed are zero. The equilibrium energy is –7.37563 eV/atom and nearest neighbor bond length 1.45 Å. For an assumed layer thickness of 3.4 Å, which is the standard layer separation thickness for graphite, the effective Young's modulus from the bulk is $Y =$ 1.261 TPa with an effective Poisson's ratio of 0.302. These values agree well with measured values for graphite and carbon nanotubes [23].

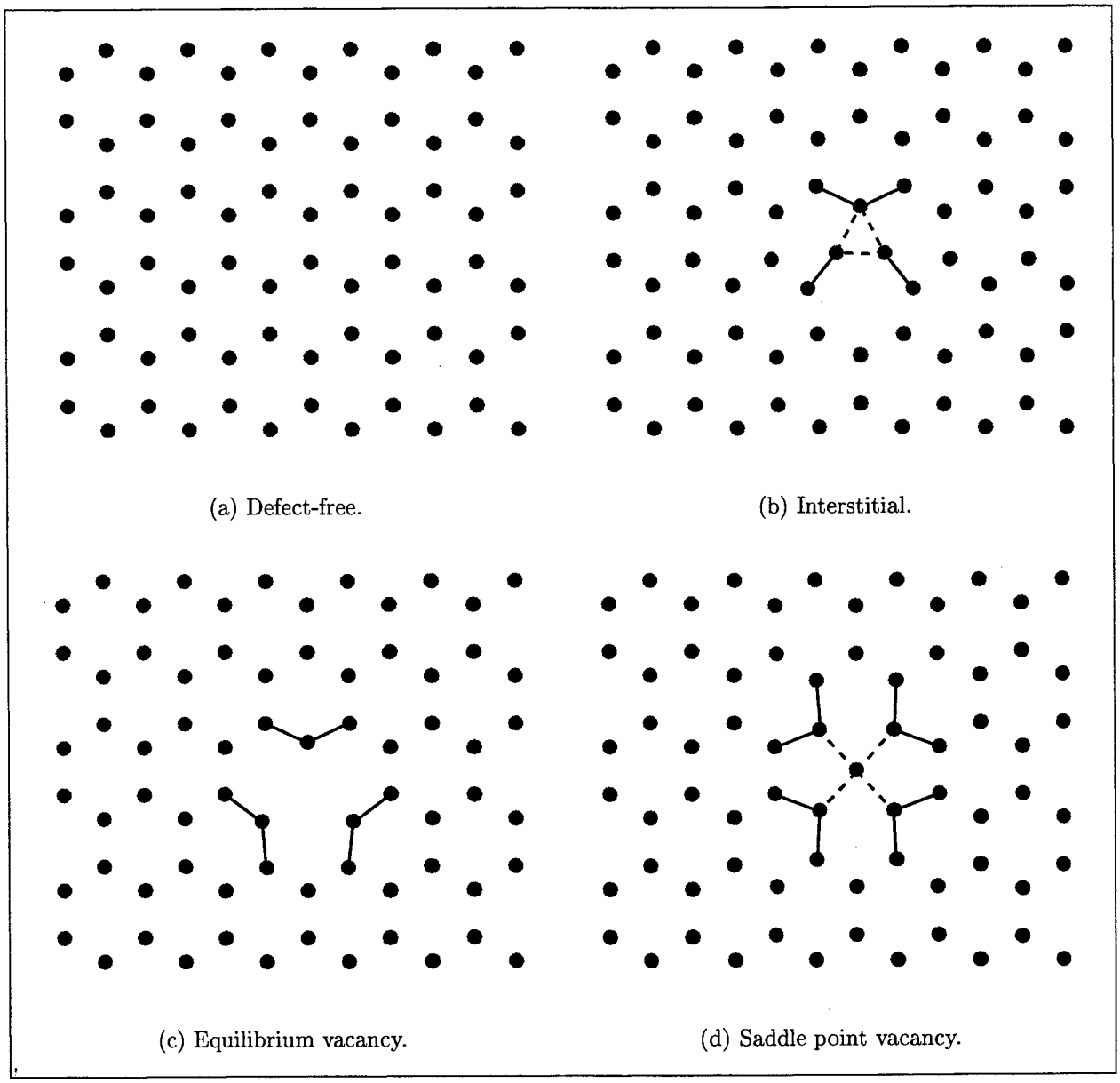

(a) Defect-free.

(b) Interstitial.

(c) Equilibrium vacancy.

(d) Saddle point vacancy.

Figure 8. Atom configurations in periodic cell. Lines are used to denote regions near the defect.

The model problem solved at the macroscopic scale is depicted in Figure 9. The uniform grid is composed of 25 4-noded quadrilateral elements. The right edge is pulled uniformly and the left edge is held fixed. All units of measure are carried through in terms of eV and Å so that no assumption of a layer thickness is required. That is, although the problem is

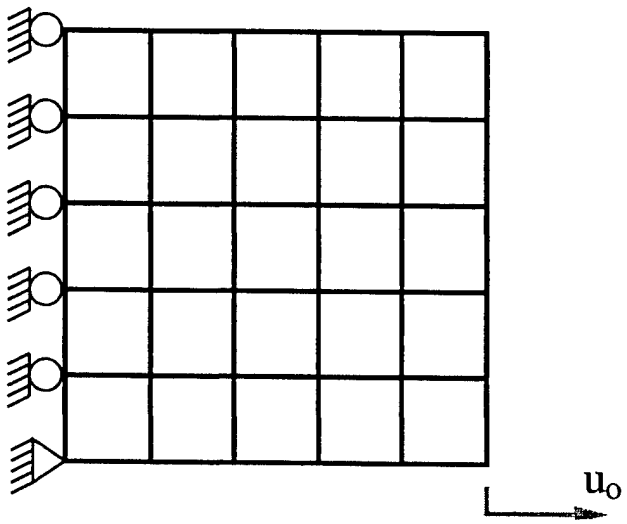

Figure 9. FE model of macroscopic problem.

two-dimensional, there is no need for a plane assumption.

The solution procedure involves application of incremental loads with iterative loops over equation (47) and sub-loops over (43). The sub-loops seek converged values for $\mathbf{v}^{[1]}$ subject to the modification from equation (33). In this problem, an overly cautious load increment of 1.0×10^{-4} strain was used, which ensured convergence tolerances for both $\mathbf{v}^{[0]}$ and $\mathbf{v}^{[1]}$ far beyond 10^{-8}Å.

The effective strain energy density and material properties are shown vs. strain in Figures 10 and 11. Of key interest are the sudden jumps that occur for the effective material properties of saddle point and interstitial defect scenarios at approximate strain values of 0.05 and 0.15, respectively. This is attributable to the relative instability of those types of point defects. Such observations were made previously for the saddle point vacancy in [20]. The effective properties and energies at larger strains after the initial instability are meaningless and are therefore not shown. The instability occurs in this problem because the separation distance between neighboring atoms near the point defect exceeds the cut-off radius of the potential because of the deformation, thereby distorting the strain energy and effective properties.

We expect that the actual strain is much smaller before the instability occurs because of the present zero-temperature assumption.

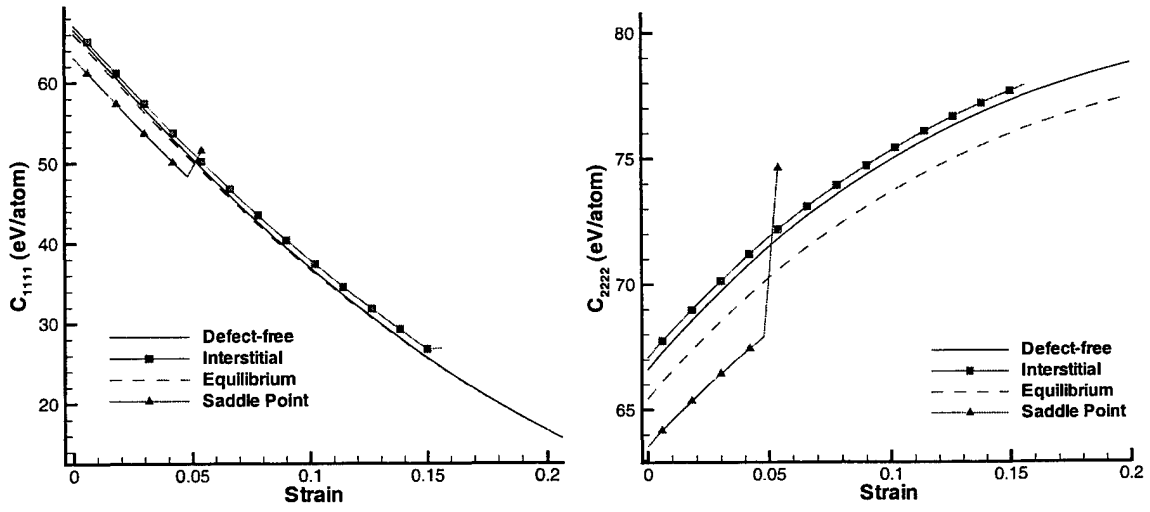

(a) C_{1111} (b) C_{2222}

Figure 10. Material property change with applied uniform strain.

It is noteworthy that the approximate atom density in the longitudinal direction decreases (cell elongates), while it increases in the transverse direction. The subsequent material nonlinear effect causes the properties to decrease in C_{1111} while increase in C_{2222}. We also note that the interstitial point defect possesses the highest values for material properties and lowest strain energy, whereas the trends for the saddle point vacancy are precisely the reverse. The defect-free structure exhibits stronger material properties and higher strain energy than the equilibrium vacancy structure.

Comparing convergence rates between methodologies with homogenization (i.e., $\mathbf{v}^{[1]} \neq 0$) and without homogenization (i.e., $\mathbf{v}^{[1]} = 0$) shows the former with a distinct advantage.*

*The methodology without homogenization implies an approach whose material property tensor is computed directly from the second derivative of the energy potential and whose formulation does not involve a perturbative term.

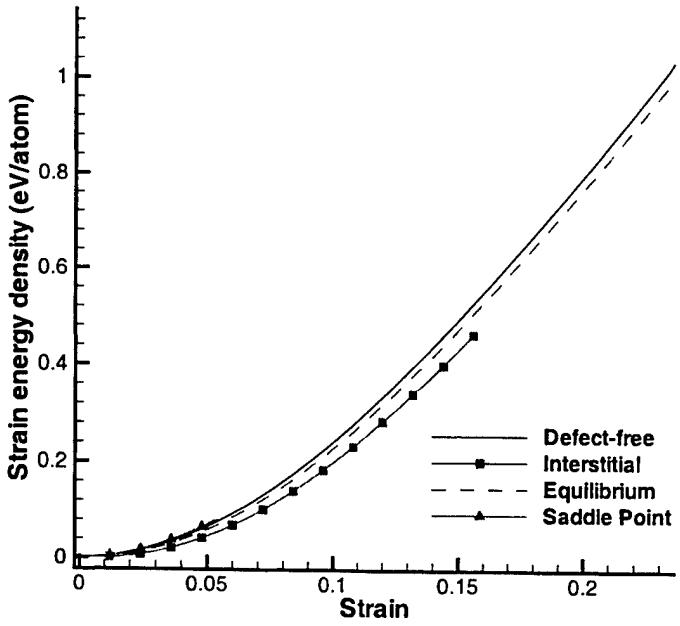

Figure 11. Strain energy with applied uniform strain.

The equilibrium vacancy configuration is used here. The convergence results are illustrated in Figure 12. The calculation is of the transverse displacement of the upper right corner node of the mesh in Figure 9 as it evolves with the total number of computation cycles, N_{steps}. The computation cycle is computed by adding the total number of nonlinear iterations steps (major loops plus sub-loops) with the total number of load increments, which is a crude way to estimate the convergence behavior. The number of load increments is selected to ensure that the final transverse displacement in the two methods is less than 1% different in magnitude. Figure 12 shows that the total required number of calculation steps is smaller in the homogenization result by a factor of four.

This convergence behavior is attributable to the addition of the $\mathbf{v}^{[1]}$ term in equation (33), which is closer to the energy minimizing configuration than equation (32) alone. Figure 13 illustrates the atom displacement due to equation (32) relative to a local coordinate

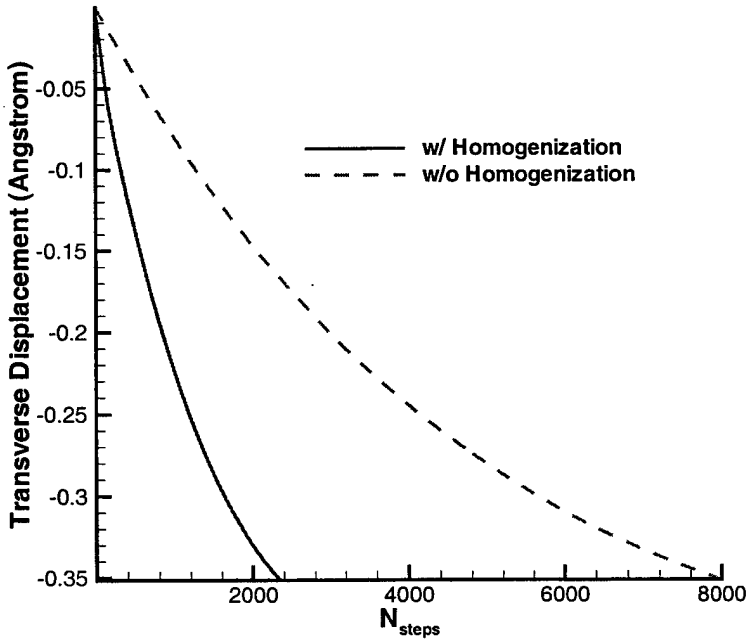

Figure 12. Convergence with and without homogenization.

system centered on the periodic cell, and Figure 14 illustrates the subsequent correction from equation (33).

The uniform strain applied in this example results in a uniform state of strain throughout the entire mesh in Figure 9. It should be noted that more complex loading scenarios can be treated merely by changing the boundary conditions of the problem. These simple results, however, are indicative of the generality of the method for two- and three-dimensional problems.

8. Conclusions

Linking atomic scale physics with continuum scale phenomena is of keen interest in the mechanical study of solids and nanostructures. The effects that dominate the mechanical

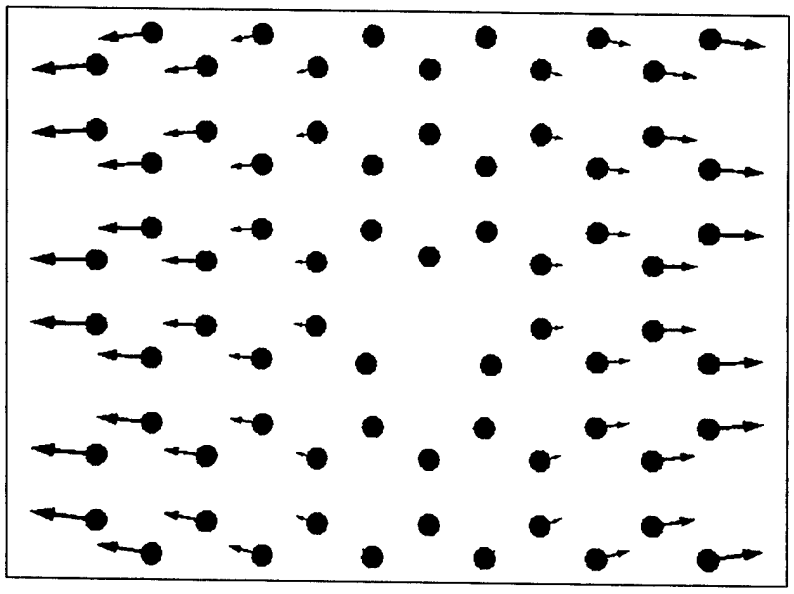

Figure 13. Atom displacements due to global deformation.

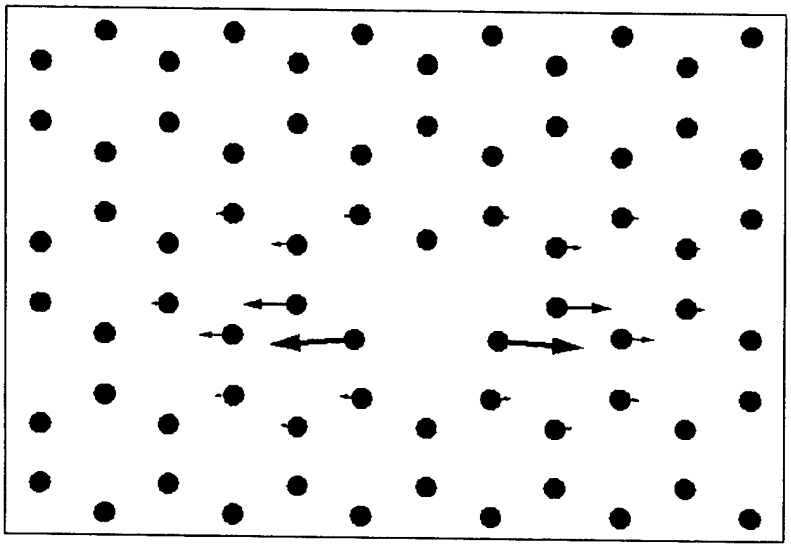

Figure 14. Atom displacements due to homogenization method.

behavior at the continuum scale typically initiate and evolve from the atomic scale. Moreover, periodic structures can emanate from nanopatterning and epitaxy through stresses induced from an underlying substrate. Despite numerous promising methods in the literature that are capable of linking scales up to the micron level, periodic structures with global dimensions

at and beyond the millimeter range – needed for mass producing nanoscale devices – have only begun to be studied. To this end, we have attempted to address this issue by exploiting the features of homogenization theory to devise a scheme that passes atomistic information to very large continuum scales.

We have applied the Cauchy-Born rule to the atom scale by assuming that the configuration of atoms used to solve for the perturbation displacement at each load increment is indeed the minimizing configuration of the atomistic energy. We have not considered the method in conjunction with a lattice statics routine, i.e., various strategies of minimizing the atomistic energy by quenched molecular dynamics or solving Newton's equations to minimize the interatom forces. These assumptions (i.e., zero temperature and Cauchy-Born) also preclude the formulation from modeling thermally activated phenomena such as crack growth, propagation, or damage evolution. However, it can be used to estimate mechanical effects across coupled length scales and, if needed, serve as the underlying framework for modified algorithms that can account for such problems.

We demonstrated the method for one- and two-dimensional problems containing point defects. Mechanical data were reported from numerical experiments. The paucity of experimental data for nanomechanics makes validation difficult. However, the material properties stemming from the reference configuration compares very well with available published measurements and the observed trends from mechanical deformation agree with generally accepted intuition.

For this work, the specific case of the Tersoff-Brenner Type II potential was considered. But the principles and the general equations can be extended to any potential, provided the appropriate derivatives can be obtained as in [14]. Typically for classical systems, onerous tensor algebra and calculus are required or more computationally efficient procedures can be implemented to obtain derivatives numerically [24].

The aim of this report was to describe an approach by which atomistic physics can be embedded into a continuum formulation for large scale systems. This goal has been achieved by formulating a consistent set of equations involving a classical atomistic potential at the fine scale and general finite strain and deformation elasticity at the coarse scale. Simple 1-D analytical results and 2-D numerical experiments were shown to illustrate the approach and its features. More realistic multiaxial problems in two and three dimensions for more detailed validation are the subjects of ongoing work.

9. References

[1] De Rosa, C., C. Park, E. L. Thomas, and B. Lotz. "Microdomain Patterns From Directional Eutectic Solidification and Epitaxy." *Nature*, vol. 405, pp. 433–437, 2000.

[2] Komori, F., S. Ohno, and K. Nakatsuji. "Arrays of Magnetic Nanodots on Nitrogen-modified Cu(001) Surfaces." *Journal of Physics: Condensed Matter*, vol. 14, pp. 8177–8197, 2002.

[3] Strobel, M., K.-H. Heinig, and T. Michely. "Mechanisms of Pit Coarsening in Ion Erosion of fcc(111) Surfaces: A Kinetic 3-D Lattice Monte-Carlo Study." *Surface Science*, vol. 486, pp. 136–156, 2001.

[4] Sinclair, J. "Improved Atomistic Model of a bcc Dislocation Core." *Journal of Applied Physics*, vol. 42, pp. 5321–5329, 1971.

[5] Mullins, M., and M. A. Dokainish. "Simulation of the (001) Plane Crack in α-Iron Employing a New Boundary Scheme." *Philosophical Magazine A*, vol. 46, pp. 771–787, 1982.

[6] Cleri, F., S. R. Phillpot, D. Wolf, and S. Yip. "Atomistic Simulations of Materials Fracture and the Link between Atomic and Continuum Length Scales." *Journal of the American Ceramic Society*, vol. 81, pp. 501–516, 1998.

[7] Tadmor, E. B., M. Ortiz, and R. Phillips. "Quasicontinuum Analysis of Defects in Solids." *Philosophical Magazine A*, vol. 73, no. 6, pp. 1529–1563, 1996.

[8] Broughton, J. Q., F. F. Abraham, N. Bernstein, and E. Kaxiras. "Concurrent Coupling of Length Scales: Methodology and Application." *Physical Review B*, vol. 60, no. 4, pp. 2391–2403, 15 July 1999.

[9] Rudd, R. E., and J. Q. Broughton. "Concurrent Coupling of Length Scales in Solid State Systems." *Physica Status Solidi B - Basic Research*, vol. 217, no. 1, pp. 251–291, January 2000.

[10] Bensoussan, A., J. L. Lions, and G. Papanicolaou. *Asymptotic Analysis for Periodic Structures*. Amsterdam: North-Holland, 1978.

[11] Sanchez-Palencia, E. *Non-homogeneous Media and Vibration Theory: Lecture Notes in Physics*. vol. 127. Berlin: Springer-Verlag, 1980.

[12] Bakhvalov, N., and G. Panasenko. *Homogenization: Averaging Processes in Periodic Media*. Dordrecht, The Netherlands: Kluwer, 1989.

[13] Ericksen, J. L. *Phase Transformations and Material Instabilities in Solids*, Orlando: Academic Press, Inc., pp. 61–77, 1984.

[14] Chung, P. W., and R. R. Namburu. "Multiscale Methodology: From Atoms to Continuum." ARL-TR-2645, U.S. Army Research Laboratory, Aberdeen Proving Ground, MD, 2002.

[15] Marsden, J. E., and T. J. R. Hughes. *Mathematical Foundations of Elasticity*. New York: Dover Publications, Inc., 1983.

[16] Mura, T. *Micromechanics of Defects in Solids*. Dordrecht, The Netherlands: Martinus Nijhoff Publishers, 1987.

[17] Takano, N., Y. Ohnishi, M. Zako, and K. Nishiyabu. "The Formulation of Homogenization Method Applied to Large Deformation Problem for Composite Materials." *International Journal of Solids and Structures*, vol. 37, pp. 6517–6535, 2000.

[18] Tersoff, J. "Empirical Interatomic Potential for Carbon, With Applications to Amorphous Carbon." *Physical Review Letters*, vol. 61, no. 25, pp. 2879–2882, 19 December 1988.

[19] Brenner, D. W. "Empirical Potential for Hydrocarbons for Use in Simulating the Chemical Vapor Deposition of Diamond Films." *Physical Review B*, vol. 42, no. 15, pp. 9458–9471, 15 November 1990.

[20] Kaxiras, E., and K. C. Pandey. "Energetics of Defects and Diffusion Mechanisms in Graphite." *Physical Review Letters*, vol. 61, no. 23, pp. 2693–2696, 1988.

[21] Hjort, M., and S. Stafström. "Modeling Vacancies in Graphite via the Hückel Method." *Physical Review B*, vol. 61, no. 20, pp. 14089–14094, 2000.

[22] Krasheninnikov, A. V., K. Nordlund, and J. Keinonen. "Production of Defects in Supported Carbon Nanotubes Under Ion Irradiation." *Physical Review B*, vol. 65, pp. 165423–165431, 2002.

[23] Krishnan, A., E. Dujardin, T. W. Ebbesen, P. N. Yianilos, and M. M. J. Treacy. "Young's Modulus of Single-Walled Nanotubes." *Physical Review B*, vol. 58, no. 20, pp. 14013–14019, 1998.

[24] Allen, M. P., and D. J. Tildesley. *Computer Simulation of Liquids*. Oxford: Clarendon Press, 1987.

Report Documentation Page

Form Approved
OMB No. 0704-0188

1. REPORT DATE *(DD-MM-YYYY)*	2. REPORT TYPE	3. DATES COVERED (From - To)
December 2002	Final, December 2002	November 2001–November 2002

4. TITLE AND SUBTITLE
Computational Method for Atomistic-Continuum Homogenization

5a. CONTRACT NUMBER

5b. GRANT NUMBER

5c. PROGRAM ELEMENT NUMBER

6. AUTHOR(S)
Peter W. Chung, Raju R. Namburu, Charles Cornwell*, Brian J. Henz, and Jerry A. Clarke

5d. PROJECT NUMBER
DR1-FY02-CIS-01

5e. TASK NUMBER

5f. WORK UNIT NUMBER

7. PERFORMING ORGANIZATION NAME(S) AND ADDRESS(ES)
U.S. Army Research Laboratory
ATTN: AMSRL-CI-HC
Aberdeen Proving Ground, MD 21005-5067

8. PERFORMING ORGANIZATION REPORT NUMBER
ARL-TR-2894

9. SPONSORING/MONITORING AGENCY NAME(S) AND ADDRESS(ES)

10. SPONSOR/MONITOR'S ACRONYM(S)

11. SPONSOR/MONITOR'S REPORT NUMBER(S)

12. DISTRIBUTION/AVAILABILITY STATEMENT
Approved for public release; distribution is unlimited.

13. SUPPLEMENTARY NOTES
*High Performance Technologies, Inc., Aberdeen Office, 1201 Technology Drive, Suite 206, Aberdeen, MD 21001

14. ABSTRACT
The homogenization method is used as a framework for developing a multiscale system of equations involving atoms at zero temperature at the small scale and continuum mechanics at the very large scale. The Tersoff-Brenner Type II potential (Tersoff, J. "Empirical Interatomic Potential for Carbon, With Applications to Amorphous Carbon." *Physical Review Letters*, vol. 61, no. 25, pp. 2879–2882, 19 December 1988; Brenner, D. W. "Empirical Potential for Hydrocarbons for Use in Simulating the Chemical Vapor Deposition of Diamond Films." *Physical Review B*, vol. 42, no. 15, pp. 9458–9471, 15 November 1990) is employed to model the atomic interactions while hyper elasticity governs the continuum. A quasi-static assumption is used together with the Cauchy-Born approximation of enforce the gross deformation of the continuum on the positions of the atoms. The two-scale homogenization method establishes coupled self-consistent variational equations in which the information at the atomistic scale, formulated in terms of the Lagrangian stiffness tensor, concurrently feeds the material information to the continuum equations. Analytical results for a one-dimensional molecular wire and numerical experiments for a two-dimensional graphene sheet demonstrate the method and its applicability.

15. SUBJECT TERMS
homogenization, numerical methods, multiscale, computational mechanics, graphite, lattice mechanics

16. SECURITY CLASSIFICATION OF:			17. LIMITATION OF ABSTRACT	18. NUMBER OF PAGES	19a. NAME OF RESPONSIBLE PERSON
a. REPORT	b. ABSTRACT	c. THIS PAGE			Peter Chung
UNCLASSIFIED	UNCLASSIFIED	UNCLASSIFIED	UL	43	19b. TELEPHONE NUMBER *(Include area code)* 410-278-6027